applied sciences

IMPACT FACTOR 2.838

CITESCORE 3.7

Article

Identifying Brain Abnormalities with Schizophrenia Based on a Hybrid Feature Selection Technology

Chen Qiao, Lujia Lu, Lan Yang and Paul J. Kennedy

Special Issue
Optical Methods for Tissue Diagnostics

Edited by
Dr. Nikolaos Kourkoumelis and Dr. Edgar Guevara

MDPI

https://doi.org/10.3390/app9102148

applied sciences

MDPI

Article

Identifying Brain Abnormalities with Schizophrenia Based on a Hybrid Feature Selection Technology

Chen Qiao [1,*], Lujia Lu [1], Lan Yang [1] and Paul J. Kennedy [2]

[1] School of Mathematics and Statistics, Xi'an Jiaotong University, Xi'an 710049, China; luke2016@stu.xjtu.edu.cn (L.L.); yanglan2018@stu.xjtu.edu.cn (L.Y.)

[2] Center for Artificial Intelligence, University of Technology Sydney, Sydney 2007, Australia; Paul.Kennedy@uts.edu.au

* Correspondence: qiaochen@xjtu.edu.cn; Tel.: +86-029-82660949

Received: 17 April 2019; Accepted: 16 May 2019; Published: 26 May 2019

Featured Application: The hybrid feature selection method, which combines both machine learning and traditional statistical methods, is proposed to identify the brain abnormalities of schizophrenia. The results suggest that the brain regions and connectivity in SZs are destroyed compared with HCs, which may cause the cognitive deficits and autistic thinking in SZs. The findings support the validation of the proposed hybrid feature selection method, and thus, it is promised that such a hybrid feature selection method can be further used for other kinds of medical data analysis to enhance the diagnosis ability and further for precision medicine.

Abstract: Many medical imaging data, especially the magnetic resonance imaging (MRI) data, usually have a small sample size, but a large number of features. How to reduce effectively the data dimension and locate accurately the biomarkers from such kinds of data are quite crucial for diagnosis and further precision medicine. In this paper, we propose a hybrid feature selection method based on machine learning and traditional statistical approaches and explore the brain abnormalities of schizophrenia by using the functional and structural MRI data. The results show that the abnormal brain regions are mainly distributed in the supramarginal gyrus, cingulate gyrus, frontal gyrus, precuneus and caudate, and the abnormal functional connections are related to the caudate nucleus, insula and rolandic operculum. In addition, some complex network analyses based on graph theory are utilized on the functional connection data, and the results demonstrate that the located abnormal functional connections in brain can distinguish schizophrenia patients from healthy controls. The identified abnormalities in brain with schizophrenia by the proposed hybrid feature selection method show that there do exist some abnormal brain regions and abnormal disruption of the network segregation and network integration for schizophrenia, and these changes may lead to inaccurate and inefficient information processing and synthesis in the brain, which provide further evidence for the cognitive dysmetria of schizophrenia.

Keywords: magnetic resonance imaging; schizophrenia; feature selection; brain abnormalities; biomarkers

1. Introduction

Schizophrenia (SZ) is a kind of mental disorder characterized by abnormal social behaviour and a failure to understand reality. Recently, decades of research on brain structure and function have provided us with some understanding of the neurobiological mechanisms underlying its symptoms [1,2]. For example, studies on brain structure suggest that neuroanatomical alterations may underlie the clinical onset of psychotic symptoms. The findings from functional brain imaging studies support a leading hypothesis that SZ stems from disconnectivity, namely abnormal interactions

between wide-spread brain networks. Recently, neuroimaging techniques like structural magnetic resonance imaging (sMRI) and functional magnetic resonance imaging (fMRI) have become a powerful tool to examine the abnormal regions and aberrant connectivity of brain networks in SZ, which bring psychiatry from subjective descriptive classification into objective and tangible brain-based measures [3]. For example, Du et al. applied a novel group information guided method to estimate inherent dynamic functional brain networks and found that the abnormalities of SZ were mainly distributed in the cerebellum, frontal cortex, thalamus and temporal cortex [4]. With fMRI data of SZ, Shine et al. showed that dynamic changes of functional connectivity are essential for cognitive processing [5]. Rosenberg et al. demonstrated that the whole-brain functional connectivity strength might serve as a biomarker of sustained attention for both healthy and disease assessments [6]. It was shown that functional connectivity profiles can predict levels of fluid intelligence [7]. By a supervised learning strategy that fuses sMRI, as well as fMRI data, some modality-specific biomarkers of generalized cognition with SZ were identified [1]. Based on sMRI data, Palaniyappan et al. suggested that concomitant increase and decrease in grey matter occur in association with persistent negative thought disorder in clinically stable individuals with SZ [8]. These studies on developing biomarkers allow the field of imaging analysis and psychiatry to move forward.

Given that SZ is often accompanied by cognitive decline, the thorough investigation of brain dynamics, as well as brain structure in SZ seems important in order to better understand the underlying neural mechanism. However, for MRI data of SZ, they usually have a small sample size, but a large number of features, i.e., $n \ll p$, where n is the sample size and p is the number of features [9]. For such kinds of data, there still lacks a systematic methodology to study them. That is because it is too difficult to discover the potential information contained in the data from a limited number of observations, which form a cognitive concept of the data or complete identification task [10]. To deal with data of dimensions much larger than the sample size, the generally used approach is dimensionality reduction. Feature selection and feature extraction are common methods for dimensionality reduction. For feature selection, those essential features of the raw data that have the greatest contribution to distinguish different objects can be identified. Thus, by feature selection, we can enhance the interpretability of learning, which is crucial for exploring the mechanisms of why things are different. Mathematically, consider any raw data as an N-dimensional vector $X = (x_1, x_2, \cdots, x_N)^T$, from which we can select M features $\tilde{X} = (x_{R_1}, x_{R_2}, \cdots, x_{R_M})^T$ as required, where $x_{R_i}, i = 1, 2, \cdots, M$ are features chosen from $\{x_1, x_2, \cdots, x_N\}$ based on some rules R. The rule could be either of the following items. $\tilde{X}$ is the optimal choice with some evaluation indexes for classifiers; the feature subset has the lowest dimension for a given accuracy; the conditional probability distribution function for the data and that of the selected features remain the same; the error rate of the classifier would not be reduced by not increasing or decreasing the number of features. By such a selection process, we could get rid of either redundant or irrelevant features without incurring much loss of information. The distinguishing features can be found, and in this way, the dimension of data space declines, the complexity of data reduces and, especially, the performance of classification and prediction can be improved. Because of the direct interpretability of the data, feature selection is widely used in many fields such as genomics, medical image analysis, computer vision, speech recognition, computer vision, information retrieval, time series prediction [11–13], etc.

According to different ways of combining the evaluation criteria and classifiers, feature selection methods can be divided into five types, i.e., filter, wrapper, embedded, ensemble and hybrid methods [14]. Filter methods mainly depend on the attribute of features, and the evaluation criteria depend only on the original data, but not on classifiers [15]. Wrapper methods directly take the performance of the classifiers as the evaluation criterion for the selection of feature subsets; thus, the results of wrapper methods are related to specific classifiers [16]. Methods of embedding filter methods and wrapper methods are called embedded methods. For embedded methods, they are usually composed of two stages. Firstly, filter methods are used to eliminate most of the irrelevant and noise features, so as to reduce the data dimension of the subsequent search process effectively.

The second stage adopts wrapper methods to carry out the further feature selection process [17]. Ensemble methods are based on different sampling strategies to extract multiple sample sets, and then, they use a specific feature selection algorithm to obtain multiple sets of feature subsets. These feature subsets are further integrated to obtain a more stable feature subset [18]. Compared with the above three methods, the performance of the ensemble methods no longer depends merely on a single subset selected, but it is still limited since it uses only one specific feature learner. Hybrid methods can be combined with some different feature selection methods. Hybrid approaches combine two or more well-studied feature selection algorithms to form a new strategy and achieve a complementary advantage of different feature selection methods to solve a particular problem [19,20]. The hybrid approach usually capitalizes on the advantages from the sub-algorithms and therefore is more robust compared with single approaches. The feature selection techniques mentioned above have been applied to many fields of dimensionality reduction analysis [21–23]. In addition to the above five types of feature selection methods, some traditional statistical methods can also be used to reduce dimensionality, such as hypothesis testing, correlation coefficients, etc. These methods can obtain features with higher distinguishing ability, so as to improve the discriminative capacity of different classes [24,25].

Motivated by identifying biomarkers of SZ that are associated with cognitive composite ability and specific cognitive domains such as attention, working memory and verbal learning, in this paper, by proposing a hybrid feature selection method combining both machine learning and traditional statistical approaches, we explore the brain abnormalities of SZ. The data have 410 features, including both functional and structural MRI, i.e., functional network connectivity (FNC) and source-based morphometric (SBM) of 40 patients with SZ and 46 healthy controls (HCs). By applying our method to these two datasets, the results show that there exist six aberrant brain regions and 17 abnormal functional connections between the SZ group and HC group. Among our findings, there was an obvious decrease, as well as increase of both the grey matter volume and the connectivity of brain regions. The decreasing regions mainly appeared in the default mode network (DMN) and salience network (SN), e.g., the grey matter volume of precuneus (PCUN) and caudate (CAU), and the connectivity of these two brain regions, as well as insula (INS) and CAU were significantly reduced. Moreover, all connectivity corresponding with rolandic operculum and insula significantly reduced [26–31]. The significantly increased grey matter volume of brain regions was mainly distributed in frontal gyrus (FG) and supramarginal gyrus (SMG), and there also existed four with significantly increased connectivity, such as middle frontal gyrus and superior occipital gyrus, as well as middle occipital gyrus and fusiform gyrus, and the corresponding conclusion of increasing also was discussed [28,29,32]. To further confirm the significance of the selected abnormal functional connections, we also used complex network analysis. Since the level of response activity in brain regions and the ability of functional connectivity between different brain regions can reflect the degree of brain disorders, the results have the potential to provide evidence for accurate diagnosis and further for precision medicine learning of such kinds of psychiatric diseases.

2. Methodology

There are many feature selection methods based on machine learning, as well as traditional statistics. Combining both of them, especially developing a kind of hybrid feature selection method, is still worthy of study. In this section, we will introduce a hybrid feature selection method combining three kinds of machine learning methods and three kinds of statistical methods. In addition, some graph theory will be presented to verify the validation of the features selected by the proposed hybrid feature selection method.

2.1. Feature Selection Methods Based on Machine Learning

2.1.1. Feature Selection with Support Vector Machine

Support vector machine based on recursive feature elimination (SVMRFE) is a multi-variable wrapper feature selection algorithm, and it can keep relevant features and remove relatively insignificant feature variables in order to achieve higher classification performance. SVMRFE was first proposed for gene selection [33], and it has been widely applied to MRI data research, text analysis and biological information processing [34–36].

For SVMRFE, the scoring function for each feature i is defined as:

$$Score(i) = |\omega_i| \quad or \quad Score(i) = \omega_i^2 \tag{1}$$

where ω_i is the weight for feature i as obtained from the SVM training. Thus, features that contribute the most to discriminating the two classes are represented by $|\omega|$ with the highest values, and features with small scores are generally considered as noise, redundant or irrelevant to the problem. Therefore, eliminating features with smaller scores does not bring about great changes of the optimization problem, which is the essence of the algorithm [37,38]. The SVMRFE algorithm is briefly described as below.

Algorithm 1: Support vector machine based on recursive feature elimination (SVMRFE)
Input: Dataset D
Process:

1. Initialization

Let the current feature subset $Current\_D$ contain all features, and the optimal feature subset $Best\_D = \emptyset$;

2. Training the classifier

Train a SVM on the training set with the $Current\_D$, and evaluate the classification accuracy on the test set;

3. Updating $Current\_D$

Calculate the importance of each feature in $Current\_D$ by the scoring function (1), and eliminate features with the smallest score;

4. Updating $Best\_D$

If the accuracy rate of $Current\_D$ is greater than that of $Best\_D$, then let $Best\_D = Current\_D$;

5. Repeat Steps 2–4 until the stop condition is satisfied.

Output: The optimal feature subset $Best\_D$

The stopping criterion can be a desired dimensionality, a pre-specified number of iterations or a generalization of the performances, etc.

2.1.2. Feature Selection with Random Forest

Random forest (RF) is an ensemble machine learning method using tree-type classifiers. It is built by bootstrap sampling technology and random splitting technology, and the final classification result is made by a majority vote of the trees [39,40]. Because of its excellent generalization performance, RF is also further used for feature selection [41,42].

For a given tree, let S_0 denote the set of input predictor data vectors and S_j be the subset of the predict data reaching node j in the binary split tree. According to the performance of the current feature on node j, S_j can be divided into two subsets, i.e., S_j^L and S_j^R; here, $S_j^L \bigcup S_j^R = S_j$ and $S_j^L \bigcap S_j^R = \emptyset$. Choosing the best split according to the mean decrease of the Gini index, which is defined as:

$$\Delta Gini_i(j) = Gini(j) - (\frac{|S_j^L|}{|S_j|}Gini(j^L) + \frac{|S_j^R|}{|S_j|}Gini(j^R)) \quad (2)$$

where $Gini(j) = 1 - \sum_{c \in C} P_c^2$ is the Gini index at node j. This metric reflects the contribution of each feature to node j; therefore, we can get an estimate of feature i with Gini importance:

$$Score_{Gini}(i) = \frac{1}{n_{tree}} \sum_{t=1}^{n_{tree}} \sum_{j} \Delta Gini_i(j,t) \quad (3)$$

where $\Delta Gini_i(j,t)$ is the value of $\Delta Gini_i(j)$ on one tree t. The Gini importance indicates how large its overall discriminative value is for the classification task. We randomly chose a feature i, calculated its Gini importance defined in (4) and removed the features with Gini importance below feature i. The algorithm for feature section with random forest by Gini importance (RFFS-GI) is briefly described as below.

Algorithm 2: Feature section with random forest by Gini importance (RFFS-GI)
Input: Dataset D;
Process:
1. Randomly choose a feature i into the feature set;
2. Calculate the Gini importance of all features in the feature set with the scoring function (3);
3. Keep features with Gini importance above that of the feature i;

Output: Optimal feature subset

In addition, for bootstrap sampling technology, about 1/3 of the samples will not be collected at the end, and they are called the out of bag (OOB) data [43]. The role of OOB data can be considered as equivalent to the test data. Therefore, we can also use the classification accuracy of the random forest classifier on the OOB data as the feature separability criterion, so as to calculate the importance of each feature:

$$Score_{OOB}(i) = \sum \frac{ooberr2 - ooberr1}{N} \quad (4)$$

where $ooberr1$ is the classification error of the OOB data, $ooberr2$ is the classification error of the OOB data with adding noise on feature i and N indicates the number of trees in a random forest. We can understand that if a feature is randomly disturbed, the classification error of the OOB data will increase greatly, and it can be considered that this feature has a great influence on the classification result. The algorithm of feature section with random forest by the classification accuracy on the OOB data (RFFS-OOB) is briefly described as below.

Algorithm 3: Feature section with random forest by the classification accuracy on the OOB data (RFFS-OOB)
Input: Dataset D
Process:
1. Generate random forest;
2. Calculate feature importance based the scoring function (4), and sort the scores;
3. The top ranked features are selected as the optimal feature subset.

Output: Optimal feature subset.

In order to improve the accuracy of feature selection results for the SBM and FNC data, we used SVMRFE, RFFS-GI and RFFS-OOB, and repeated them 20 times separately, counted the frequency of the selected features by each feature selection method and integrated the optimal feature subsets.

2.2. Feature Section Based on Statistical Methods

For classical statistical methods, the discriminative ability of a feature can be quantitatively measured by its contribution on distinguishing different classes [25,44].

The Kendall tau correlation coefficient provides a distribution-free test of independence between two variables. The Kendall tau correlation coefficient of feature j can be defined as:

$$\tau_j = \frac{n_c - n_d}{n_1 \times n_2} \tag{5}$$

where n_c and n_d are the numbers of concordant and discordant pairs, respectively, and n_1 and n_2 correspond to the number of two classes of samples, respectively. For a pair of data (x_{ij}, y_i) and (x_{kj}, y_k) of feature j, it is a concordant pair when $sgn(x_{ij} - x_{kj}) = sgn(y_i - y_k)$, where $sgn()$ is the signum function (i.e., $sgn(x) = -1$ with $x < 0$, $sgn(x) = 0$ with $x = 0$ and $sgn(x) = 1$ with $x > 0$). Correspondingly, it is a discordant pair when $sgn(x_{ij} - x_{kj}) = -sgn(y_i - y_k)$. The discriminative power of each feature j is defined as the absolute value of its Kendall tau correlation coefficient.

The permutation test is a non-parametric test method, which is suitable for the case of a small sample size and unknown sample distribution. Assume that there are two samples x_A and x_B, and $\bar{x}_A$ and $\bar{x}_B$ denote the corresponding sample mean, say n_A and n_B are the corresponding sample size. At first, we calculate the observed test statistic $T_{obs} = \bar{x}_A - \bar{x}_B$. Then, the two samples are merged and divided into two groups with size n_A and n_B. For each division, the difference between the mean values of the two groups is calculated and recorded. The calculated difference set is the accurate distribution of the difference under the null hypothesis. Finally, the ratio of the absolute value of the calculated difference greater than or equal to the absolute value of T_{obs} is the p-value based on the two-sided test.

By the two-sample t-test, we can also determine whether there are significant differences of each feature. The t-value of the feature j can be defined as:

$$t_j = \frac{|\bar{x}_1 - \bar{x}_2|}{\sqrt{\frac{(n_1-1)s_1^2+(n_2-1)s_2^2}{n_1+n_2-2} \cdot (\frac{1}{n_1} + \frac{1}{n_2})}} \tag{6}$$

where $\bar{x}_1$ and $\bar{x}_2$ are the means of feature j of patients and health controls (HCs) and s_1 and s_2 represent the corresponding standard deviations. With the Kendall tau correlation coefficient, permutation test and two-sample t-test, we can identify features with significant differences.

2.3. Hybrid Feature Selection Based on Both Machine Learning and Statistical Methods

By combining the above machine learning methods and statistical methods, we propose a hybrid feature selection approach. In more detail, for machine learning methods, we summed the frequencies of SVMRFE, RFFS-GI and RFFS-OOB, then we selected the features with total frequency greater than a given value b to obtain the significant feature subset. At the same time, we selected features with the absolute values of the Kendall correlation coefficient greater than a given value c and those with the p-value of two-sample t-test, as well as that of the permutation test less than 0.05 as the significant feature subset, respectively. Finally, we integrated the significant feature subset from both the machine learning and statistical method as the optimal feature subset. The above process is a hybrid feature selection procedure, and the flowchart is shown in the Figure 1. The experiment results will show that the proposed hybrid feature section method is an effective attempt to combine machine learning and the statistical methods.

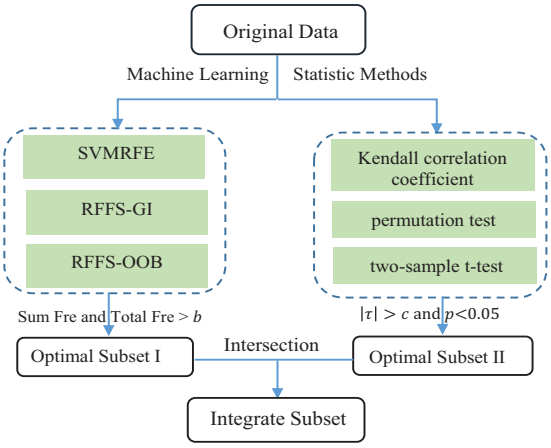

Figure 1. The flowchart of the hybrid feature selection method. Fre denotes frequency, τ the Kendall correlation coefficient, p the p-values of test and b and c the given constants. In which, SVMRFE refers to support vector machine based on recursive feature elimination, RFFS-GI refers to the feature selection with random forest by Gini importance and RFFS-OOB refers to the feature selection with random forest by the classification accuracy on the OOB data.

2.4. Complex Network Analysis Based on Graph Theory

The data we used here are a type of MRI data, which contain both the regions and the functional connection information of brains. The hybrid feature selection method can be directly used to explore the disease-related abnormal brain regions and abnormal function connections. Furthermore, since the completion of various tasks allocated for brains is implemented by the coordination and cooperation between various brain regions, so it is necessary to discover the connection networks of brains in depth.

The analysis of complex network properties by several indexes (see Figure A1) can characterize the topological attributes of the network; for example, the clustering coefficient quantifies the functional segregation of the brain network, in which the functional segregation reflects the ability of a specialized process to occur within some densely-interconnected groups of the brain regions. The length of characteristic path quantifies the functional integration of the brain network, and the functional integration reflects the ability to combine rapidly some specialized information from distributed brain regions [45]. Both global and local network efficiencies quantify the transmission capability of the brain network, and the transmission capability reflects the ability of transmitting information between different brain regions in the brain network. The main difference is that the global network efficiency focuses on the global brain network, but the local network efficiency just focuses on the local brain network. Thus, by complex network analysis, we can confirm the significance of those selected abnormal connection features and can further explore the mechanism of SZ.

3. Experiments

In this section, based on the hybrid feature selection method and network topological analysis, we located the brain abnormalities of both regions and connections with SZ. Firstly, by the SVMRFE, RFFS-GI, RFFS-OOB, correlation coefficient and hypothesis test, the candidates of brain regions and connections associated with SZ were selected separately, and then, by the hybrid method, we could confirm the significant regions and connections of SZ. Furthermore, the complex network analysis based on graph theory was used to verify the selected abnormal connections. Ultimately, we could locate some of the abnormal brain regions and abnormal connections with SZ, which provided theoretical guidance for the rapid and accurate diagnosis of psychiatric diseases and adjuvant therapy.

3.1. Data Collection and Preprocessing

In this study, the Machine Learning for Signal Processing (MLSP) 2014 Schizophrenia classification challenge data were used. The data can be download from https://www.kaggle.com/c/mlsp-2014-mri. They were collected on a 3T MRI scanner at the Mind Research Network and funded by the Centers of Biomedical Research Excellence. Image preprocessing was performed using statistical parametric mapping software (SPM, http://www.fil.ion.ucl.ac.uk/spm). Further feature extraction was done by the GIFT Toolbox (http://mialab.mrn.org/software/gift/), yielding different imaging modalities, i.e., SBM and FNC features for structural MRI and resting state functional MRI, correspondingly.

The data consisted of 40 patients with SZ and 46 HCs. A diagnosis of SZ was made by using the Structured Clinical Interview for DSM-IV (SCID; Diagnostic and Statistical Manual of Mental Disorders, DSM) [46]. Each sample had 410 features (32 for SBM and 378 for FNC). SBM features were weights of brain regions, and they indicated the concentration of grey matter in different regions of the subject's brain [47]. FNC features were the pair-wise correlation values between the time-courses of 28 brain regions and can be seen as a functional modality feature describing the subjects' overall level of synchronicity between brain areas [48]. These 28 brain regions were selected according to the anatomical automatic labeling (AAL) template, and they are shown in Figure A2, while the connections between the brain regions corresponding to these FNC features are shown in Figure A3.

3.2. Locating the Abnormalities in Brains for SZ

For both the FNC and SBM data, we performed feature selection methods based on machine learning and statistical approaches, respectively. By the hybrid process, the key features can be selected; namely for SBM data, we obtained the abnormal brain region, and for FNC data, the abnormal connectivities were achieved. Further, we used the brain network based on graph theory to analyse the selected abnormal connections. The following Figure 2 shows the whole flowchart of the procedure.

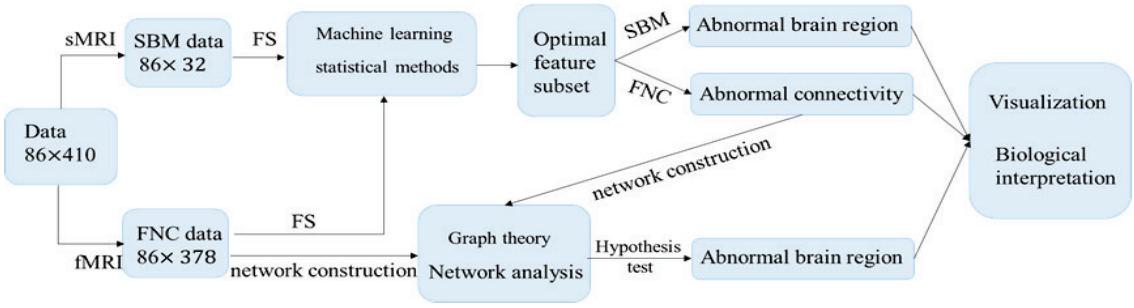

Figure 2. The flowchart of locating the abnormalities in brains for SZ. Where SBM refers to source-based morphometric, FNC refers to functional network connectivity and FS refers to feature selection.

3.2.1. Feature Selection Results Based on Machine Learning Methods

SVMRFE, RFFS-GI and RFFS-OOB were applied to perform feature selections on the MRI data respectively, with each method being repeated 20 times. Since these three methods were implemented based on the classification results and SBM data and FNC data had different classification performance, therefore, in order to obtain the key features of the two types of data more clearly, we selected the features of both of them separately. By the three feature selection methods, the results of the frequency of each feature that has been selected are shown in Figures 3 and 4 and Figures A4–A7.

It is generally believed that if the frequency of occurrence of a feature is too low, then the feature is not significant. Therefore, we only considered features with a higher frequency to obtain the significant feature subset. In Figure A8, the corresponding characteristic frequency distribution with a frequency greater than or equal to 50 is shown. Each point in this figure corresponds to the number of features with a frequency of occurrence greater than or equal to x. Further, we selected features with a frequency greater than or equal to 55, which is a balance between the numbers of features and the frequency

(the details can be found in the illustration of Figure A8). From Figures 3 and 4 and Figures A4 and A7, we can obtain the features of SBM data that are significant for distinguishing the HCs and SZ, and the corresponding indexes were 3, 7, 11, 24, 26, 30 and 32. We can also obtain the discriminative features of FNC data with indexes 244, 295, 183, 243, 33, 37, 40, 189, 220, 48, 78, 279, 353, 13, 185, 211, 265, 292, 328, 337 and 165.

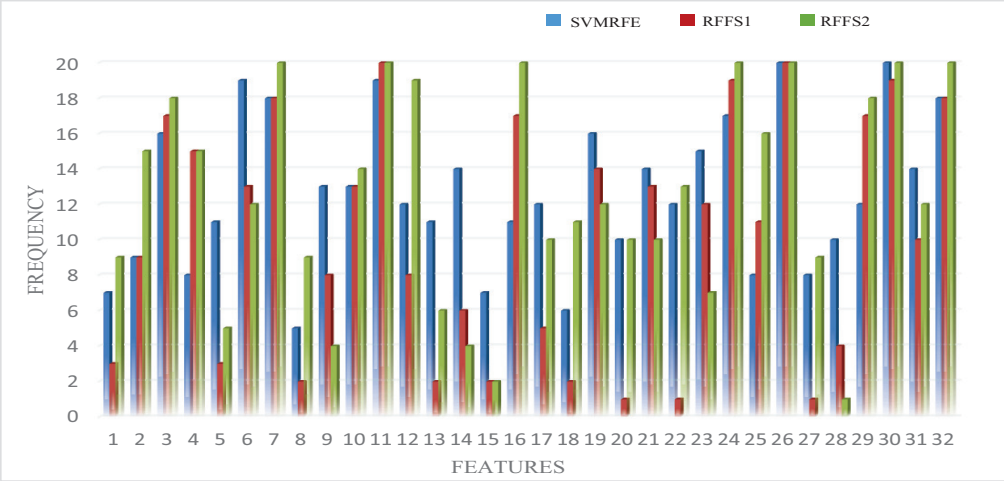

Figure 3. SVMRFE, RFFS-GI and RFFS-OOB results of SBM data.

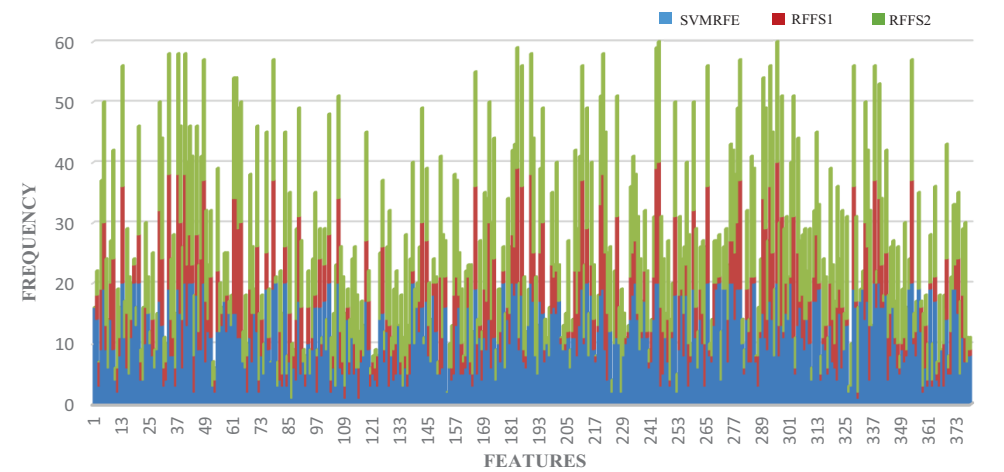

Figure 4. SVMRFE, RFFS-GI and RFFS-OOB results of FNC data.

3.2.2. Feature Selection Results Based on Statistical Methods

Statistical methods were utilized to screen out features with significant differences. The results of the Kendall correlation coefficient are shown in Figure 5, and the hypothetical test results are shown in Figure 6.

We selected features with the p-value of the hypothesis test less than 0.05 and the absolute value of Kendall correlation coefficient greater than 0.26, which is a balance between the size of the selected feature subsets and their distinguishing ability of SZ. The results are shown in Figure 7, where τ is the Kendall correlation coefficient and p_1 and p_2 are the p-values of the two-sample t-test and the permutation test, respectively.

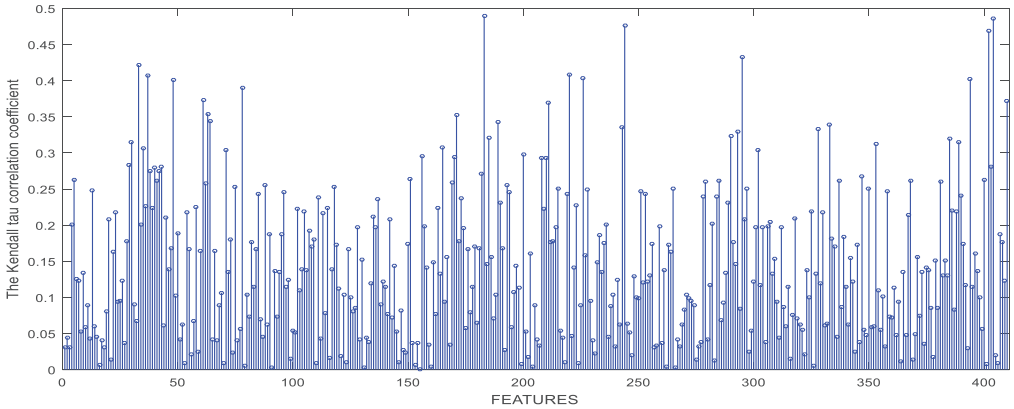

Figure 5. The results obtained by the Kendall correlation coefficient. The x axis corresponds to the features, and the y axis is the absolute value of the Kendall tau correlation coefficient.

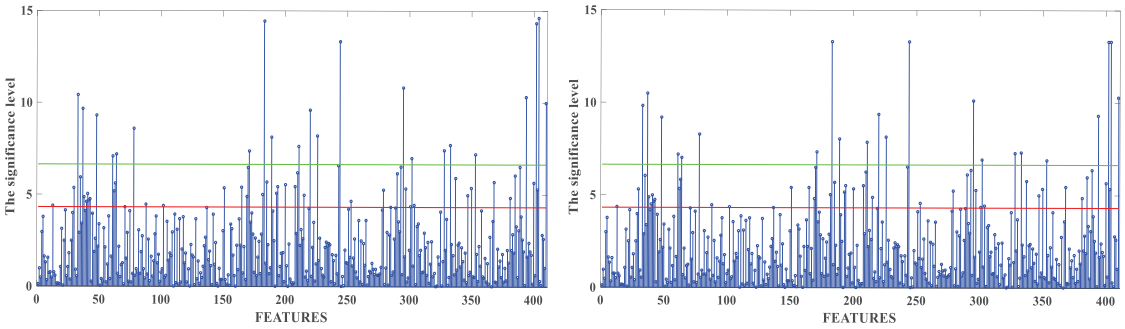

Figure 6. The results of hypothesis test for both two-sample t-tests and the permutation test. The x axis corresponds to the features, and the y axis is the significance level $(-log_2P)$. The red and green lines show the significance levels of 0.05 and 0.01, respectively. The features with $-log_2P$ values above the lines have significant differences, and they are the candidates of abnormal regions or connections.

	Fea / Value	3	7	11	16	22	24	25	26	32
SBM data	$\|\tau\|$	0.26080	0.31956	0.31522	0.40217	0.26304	0.46848	0.28152	0.4858	0.37174
	p_1	0.03503	0.01520	0.01092	0.00077	0.01964	0.00005	0.02552	0.00004	0.00098
	p_2	0.03459	0.01589	0.01209	0.00160	0.01979	0.00040	0.02469	0.00040	0.0008

	Fea / Value	33	37	40	48	61	64	78	165	171	183	185	189
FNC data	$\|\tau\|$	0.422	0.408	0.279	0.401	0.372	0.344	0.390	0.308	0.352	0.489	0.320	0.342
	p_1	0.001	0.001	0.041	0.002	0.007	0.007	0.003	0.024	0.006	0.001	0.019	0.004
	p_2	0.001	0.001	0.045	0.002	0.007	0.008	0.003	0.023	0.006	0.001	0.019	0.004
	Fea / Value	211	220	226	243	244	279	295	302	328	333	337	353
	$\|\tau\|$	0.370	0.409	0.403	0.336	0.476	0.260	0.433	0.304	0.333	0.339	0.261	0.312
	p_1	0.005	0.001	0.003	0.011	0.001	0.026	0.001	0.008	0.006	0.005	0.017	0.007
	p_2	0.004	0.002	0.004	0.011	0.001	0.027	0.001	0.008	0.006	0.006	0.018	0.008

Figure 7. Feature selection results based on statistical methods.

3.2.3. Feature Selection Results Based on a Hybrid Method

By both machine learning and statistical methods, the key candidate features for SZ were selected, and the dataset were quite similar. We adopted the intersection of them as the final selected feature subset, and thus, the abnormal brain regions from the SBM data (see Figure 8) and the abnormal functional connectivity from the FNC data (see Figure 9) can be obtained.

Machine learning	3	7	11	24	26	30	32		
Statistical methods	3	7	11	16	22	24	25	26	32
Intersection	3	7	11	24	26	32			
Brain region (abbr.)	SMG	CG	MFG	PCUN	SFG	CAU			

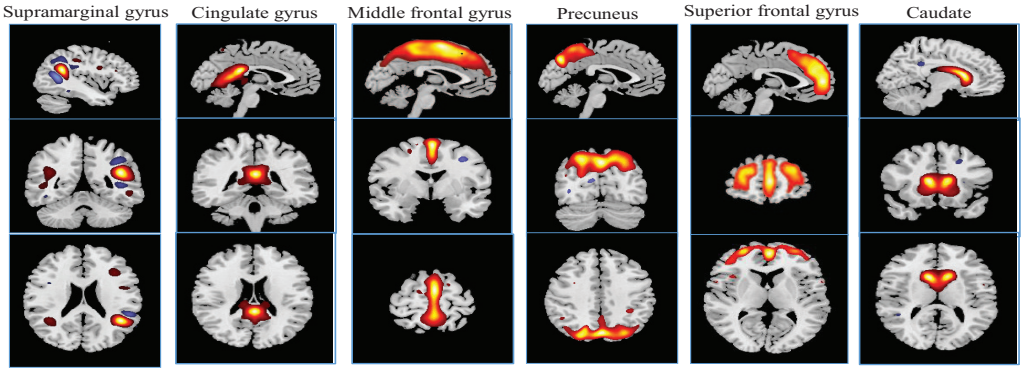

Figure 8. The selected abnormal brain regions of SZ by the hybrid method. Segall et al. presented the relationships between the cortical maps and the brain regions described by the SBM features [47].

Figure 8 shows the brain regions selected by our method that differed from healthy controls in SZ, and these abnormal brain regions were mainly distributed in supramarginal gyrus (SMG), cingulate gyrus (CG), middle frontal gyrus (MFG), precuneus (PCUN), superior frontal gyrus (SFG) and caudate (CAU). Compared with the HC group, the SZ group had significantly reduced grey matter volumes in the CG, PCUN and CAU and significantly increased grey matter volume of brain regions including SMG, MFG and SFG.

ML	SM	Intersection	Connectivity
13	33	33	17-29
33	37	37	17-48
37	40	40	17-50
40	48	48	17-71
48	61	78	7-49
78	64	165	56-42
165	78	183	29-71
183	165	185	29-42
185	171	189	46-64
189	183	211	64-59
211	185	220	64-71
220	189	243	48-39
243	211	279	59-60
244	220	295	50-71
265	226	328	68-71
279	243	337	34-71
292	279	353	52-55
295	295		
328	302		
337	328		
353	333		
	337		
	353		

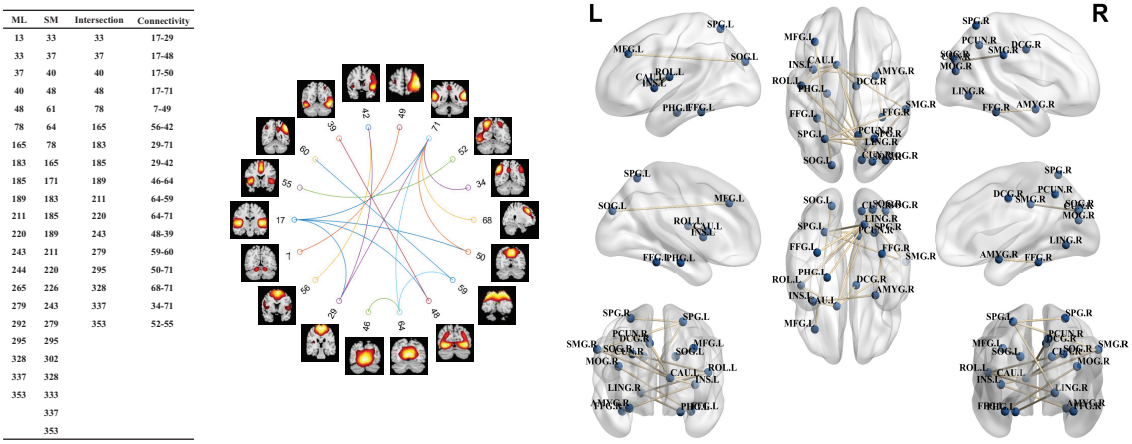

Figure 9. The abnormal functional connections of brains with SZ. In this figure, the left table lists the selected abnormal functional connections of the regions of interest (the relationships of the regions and the labels are shown in Figure A2), in which ML refers to machine learning methods and SM refers to statistical methods. The circular connectivity graph in the middle is a schematic map of the selected functional connections, which are listed in the fourth column of the left table. The labels in this graph correspond to the regions of interest, and the corresponding spatial maps of these regions (see [48]) are also shown in this graph. The right graph depicts the locations and their connections of the selected brain regions by the BrainNet Viewer toolbox [49].

Figure 9 shows that by the hybrid feature selection method proposed here, 17 abnormal functional connections between the SZ group and HC group can be discovered. Furthermore, by combining with the relationship between the connections and the regions shown in Figure A2, six connections are related to the caudate nucleus (CAU), including rolandic operculum (ROL), insula (INS), supramarginal gyrus (SMG), superior occipital gyrus (SOG), precuneus (PCUN) and median cingulate and paracingulate gyri. In addition, there also existed three abnormal functional connections related to the insula (i.e., ROL, amygdala and CAU) and four aberrant functional connection in rolandic operculum (i.e., insula, lingual gyrus, superior parietal gyrus and caudate). Among these abnormal connections discovered by our method, we can find that all connectivities corresponding with rolandic operculum and insula had significantly reduced, and these connectivities related to caudate nucleus had significantly decreased except the median cingulate and paracingulate gyri. Other than that, we also observed the significantly increased connectivity in middle frontal gyrus and superior occipital and middle occipital gyrus and fusiform gyrus, as well as left and right superior parietal gyrus. In conclusion, the brain connectivity in SZ generally decreased, but also had little increased connectivity. To show these abnormal connections more vividly, in Figure 9, we used the BrainNet Viewer toolbox to draw the precise locations of two brain regions with aberrant connections and to show the aberrant brain connectivity network in SZ [49] .

3.3. Network Evaluation

Further, to support the validity of the connectivity findings by the above hybrid feature selection method, we constructed a brain network based on these connections and explored its topological properties [50,51]. More specifically, we first chose the clustering coefficient (C), characteristic path length (L), global network efficiency (Eg) and local network efficiency ($Eloc$) as the evaluation index for each network. Then, we constructed weight networks with a threshold of one for the original and selected FNC data. At last, these four parameters of both SZ and HCs were calculated and tested by a two-sample t-test. The p-values of these four parameters were 1.70×10^{-1}, 5.02×10^{-3}, 2.99×10^{-2} and 4.27×10^{-2} for the original FNC data and 6.64×10^{-2}, 3.41×10^{-6}, 5.40×10^{-6} and 1.90×10^{-2} after feature selection by our method. Obviously, from the results of the p-values of the four parameters, we can find that the p-values of all these parameters decreased significantly after feature selection, which means that the distinction of four parameters between the HCs and SZ became more apparent after feature selection, especially the characteristic path length and the global network efficiency. This shows that the HCs and SZ become obviously distinguishable by the hybrid feature selection method and shows the validity of our method.

4. Discussion

The methods based on machine learning pay more attention to the classification accuracy, but the statistical methods emphasize the correlation between feature and label, which explains the essential difference between the two approaches. Comparing the significant subsets selected by these two approaches, it is clear that most of the biomarkers in these two subsets were same, and this means that despite the emphasis of the two approaches being different, both of them did find the significant features. Further, by integrating the significant subset of these two approaches, the significant features can be double checked and obtained finally by the hybrid method proposed in this article. For example, for the data before feature selection, the p-value of characteristic path length, which is referred to as L in the above section, was 5.02×10^{-3}. The p-value of L for the optimal subset I, which was obtained by machine learning methods, the p-value of L for the optimal subset II, which was obtained by statistic methods, and the p-value of L for the optimal subset by the proposed hybrid method were 9.40×10^{-6}, 2.82×10^{-5} and 3.41×10^{-6} respectively. The results show that the HCs and SZ became obviously distinguishable after feature selection; specially, our method was more significant than machine learning, as well as statistical methods. In summary, the hybrid method can combine the

strength of both machine learning and statistic methods to improve the accuracy of the results, and the results of network evaluation also confirmed this point.

Our findings are quite consistent with those reports that the grey matter volume of CG, PCUN and CAU is significantly reduced in SZ [26,27,52,53]. The CG is considered to be a brain region closely related to task attention, memory and affection, which has been reported to be destroyed in SZ [54]. The PCUN is the portion of the superior parietal lobule on the medial surface of each brain hemisphere, and it is often considered to be a brain region that plays an important role in the pathogenesis of SZ [55]. Given that the Behavioural Inhibition System (BIS) activity and Cloninger's Temperamental Dimension Harm Avoidance (HA) are mainly bound up with the study of the anxiety trait [56,57] and the research results show that the BIS-sensitively as well as HA are negatively correlated with the regional gray matter volume at the CG and PCUN, the SZ may be accompanied by anxiety trait due to the reduction of the gray matter volume at these two regions [58]. The CAU is one of the structures that makes up the dorsal striatum, which is a component of the basal ganglia. It can affect the cognitive function of patients, resulting in decreased memory ability, and may be the cause of cognitive dysfunction in SZ [59].

In our findings, most of the brain connectivity in SZ was significantly reduced, which had been generally accepted as the fact that the functional connectivity reduces significantly in SZ and the reduction may cause the damage of information integration [60]. Among these abnormal connectivities, CAU, INS and ROL were the most connected regions. The INS mainly participates in the formation of aversion, the regulation of pain, the production of depression, the regulation of cardiac activity and the planning of language [61], and these may be the cause of affective symptoms in SZ. Moreover, many studies have found that the connectivity in the INS decreased, which may cause the disrupted functional integration of the brain [30]. The ROL is mainly involved in language, and Wu et al. suggested that the reduction of connectivity of ROL improves the vulnerability of speech recognition to speech masking [62]. Not only that, the work also showed that the ROL is bound up with hallucination [63]. It has been reported that SZ is often accompanied by motor abnormalities, and the work showed that the abnormalities of the motor system are related to the abnormal functional connectivity of CAU and CG [64]. In addition, the work showed that the network of DMN including posterior cingulate cortex and lateral temporal cortex and SN including INS and CAU have abnormal connectivity in SZ [65]. DMN is mainly related to oriented attention and self-monitoring [66], and SN is implicated in orienting toward salient external stimuli and internal events [67]. These state clearly that the abnormal connectivity of CAU and INS may result in the cognitive deficits.

In addition to the above findings that there exist some decreasing regions and connections, we also found that there exist some increasing regions in SMG, MFG and SFG and the increasing connectivity of MFG and superior occipital gyrus, the median cingulate and paracingulate gyri and CAU, the left and right superior parietal, as well as middle occipital gyrus and fusiform gyrus. Some corresponding conclusions were also mentioned in literatures [28,29,32]. Research showed that the connectivity of the frontoparietal network (FPN) and DMN significantly increased [65]. The FPN including dorsolateral prefrontal cortex and dorsolateral parietal cortex is implicated in executive control [68], which means the function of executive control of SZ is different from HCs. In conclusion, we found that most abnormal brain regions and connectivity discovered by our method were mainly related to cognition and hallucination. These abnormalities may be the reason for the cognitive deficits and autistic thinking in SZ. Moreover, our studies show that compared with HCs, the brain network of SZ is not a single decline or rise, but a mix of both. The most abnormal connectivity may cause the information integration and transmission damage. Thus, by our method, we did find the abnormal regions and the connectivity of brain that were strongly related to SZ, and the results also supported the effectiveness of using functional disconnectivity from neuroimaging as a biomarker for diagnosis of mental disorders [69].

5. Conclusions

By the proposed hybrid feature selection approach, which combined both machine learning and traditional statistical methods, the abnormal brain regions and abnormal connections in brains of SZ were discovered. The results of SBM data showed that the abnormal brain regions of SZ were mainly distributed in supramarginal gyrus, cingulate gyrus, middle frontal gyrus, superior frontal gyrus, precuneus and caudate. These brain regions are reported to have strong association with SZ, and they are mainly involved in perception, thinking, emotion and spiritual activity. The results of FNC data showed that most of the abnormal functional connections in brains of SZ were related to FPN, DMN and SN. These three networks are closely related to cognitive deficits, especially in executive control and salience processing. All of the results suggest that the brain regions and connectivity in SZ are destroyed compared with HCs, and the abnormal activity may cause the cognitive deficits and autistic thinking in SZ. In addition, the complex network analysis further verified the significance of the selected abnormal functional connections. All findings supported the validation of the proposed hybrid feature selection method, and thus, it is promised that such a hybrid feature selection method can be further used for other kinds of medical data analysis to enhance the diagnosis ability.

Author Contributions: Conceptualization, C.Q.; methodology, C.Q. and L.L.; writing, original draft preparation, L.L. and L.Y.; writing, review and editing, C.Q. and P.J.K.; funding acquisition, C.Q.

Funding: This research was funded by NSFC Nos. 11471006 and 11101327, the Fundamental Research Funds for the Central Universities (No. xjj2017126), the Science and Technology Project of Xi'an (No. 201809164CX5JC6) and the HPC Platform of Xi'an Jiaotong University.

Conflicts of Interest: The authors declare no conflict of interest.

Appendix A

Clustering coefficient (C): Average nodal clustering coefficient.	$C = \frac{1}{n}\sum_{i\in N} C_i = \frac{1}{n}\sum_{i\in N} \frac{2t_i}{k_i(k_i-1)}$
Characteristic path length (L): integration and global routing efficiency of a network	$\frac{1}{L} = \frac{1}{n(n-1)}\sum_{i\neq j\in N} \frac{1}{d_{ij}} = \boldsymbol{E_{global}}$
Gamma (γ): the normalized clustering coefficient	$\gamma = C/C_{rand}$
Lambda (λ): the normalized characteristic path length	$\lambda = L/L_{rand}$
Sigma (σ): the extent of small-world property	$\boldsymbol{\sigma = \gamma/\lambda}$
Degree: number of links connected directly to a node	$k_i = \sum_{j\in N} a_{ij}$ / $k_i = \sum_{j\in N} w_{ij}$
Nodal clustering coefficient: local clustering and closeness of neighborhood of node	C_i
Nodal efficiency: efficiency for a node communicating with the other	$e_i = \frac{1}{n-1}\sum_{j\in N, j\neq i} \frac{1}{d_{ij}}$
Betweenness centrality: a centrality measure in the communications between other nodes	$b_i = \frac{1}{(n-1)(n-2)}\sum_{j\neq i\neq k} \frac{\sigma_{jk}(i)}{\sigma_{jk}}$

Figure A1. Different measuring parameters of the global and local network properties. Where t_i is the number of triangles around node i, d_{ij} is the shortest path length between node i and node j, C_{rand} and L_{rand} refer to the average clustering coefficient and characteristic path length values obtained from 100 random networks with the same number of nodes, as well as edges and the same degree of distribution as the original network, σ_{jk} is the number of shortest paths between j and k and $\sigma_{jk}(i)$ is the number of shortest paths between j and k that pass through i.

Labels	*Regions*	*abbr.*	*x(mm)*	*y(mm)*	*z(mm)*
21	Olfactory cortex	OLF.L	-8.06	15.05	-11.46
17	Rolandic operculum	ROL.L	-47.16	-8.48	13.95
7	Middle frontal gyrus	MFG.L	-33.43	32.73	35.46
23	Superior frontal gyrus, medial	SFGmed.L	-4.8	49.17	30.89
24	Superior frontal gyrus, medial	SFGmed.R	9.1	50.84	30.22
38	Hippocampus	HIP.R	29.23	-19.78	-10.33
56	Fusiform gyrus	FFG.R	33.97	-39.1	-20.18
29	Insula	INS.L	-35.13	6.65	3.44
46	Cuneus	CUN.R	13.51	-79.36	28.23
64	Supramarginal gyrus	SMG.R	57.61	-31.5	34.48
67	Precuneus	PCUN.L	-7.24	-56.07	48.01
48	Lingual gyrus	LING.R	16.29	-66.93	-3.87
39	Parahippocampal gyrus	PHG.L	-21.17	-15.95	-20.7
59	Superior parietal gyrus	SPG.L	-23.45	-59.56	58.96
50	Superior occipital gyrus	SOG.R	24.29	-80.85	30.59
53	Inferior occipital gyrus	IOG.L	-36.36	-78.29	-7.84
25	Superior frontal gyrus, medial orbital	ORBsupmed.L	-5.17	54.06	-7.4
68	Precuneus	PCUN.R	9.98	-56.05	43.77
34	Median cingulate and paracingulate gyri	DCG.R	8.02	-8.83	39.79
60	Superior parietal gyrus	SPG.R	26.11	-59.18	62.06
52	Middle occipital gyrus	MOG.R	37.39	-79.7	19.42
72	Caudate nucleus	CAU.R	14.84	12.07	9.42
71	Caudate nucleus	CAU.L	-11.46	11	9.24
55	Fusiform gyrus	FFG.L	-31.16	-40.3	-20.23
42	Amygdala	AMYG.R	27.32	0.64	-17.5
20	Supplementary motor area	SMA.R	8.62	0.17	61.85
47	Lingual gyrus	LING.L	-14.62	-67.56	-4.63
49	Superior occipital gyrus	SOG.L	-16.54	-84.26	28.17

Figure A2. Twenty eight brain regions selected for the experiment according to the AAL template.

Fea	R1	R2	Fea	R1	R2	Fea	R1	R2	Fea	R1	R2	Fea	R1	R2	Fea	R1	R2	Fea	R1	R2	Fea	R1	R2
1	21	17	49	17	55	97	23	71	145	38	20	193	46	59	241	67	47	289	50	25	337	34	71
2	21	7	50	17	42	98	23	55	146	38	47	194	46	50	242	67	49	290	50	68	338	34	55
3	21	23	51	17	20	99	23	42	147	38	49	195	46	53	243	48	39	291	50	34	339	34	42
4	21	24	52	17	47	100	23	20	148	56	29	196	46	25	244	48	59	292	50	60	340	34	20
5	21	38	53	17	49	101	23	47	149	56	46	197	46	68	245	48	50	293	50	52	341	34	47
6	21	56	54	7	23	102	23	49	150	56	64	198	46	34	246	48	53	294	50	72	342	34	49
7	21	29	55	7	24	103	24	38	151	56	67	199	46	60	247	48	25	295	50	71	343	60	52
8	21	46	56	7	38	104	24	56	152	56	48	200	46	52	248	48	68	296	50	55	344	60	72
9	21	64	57	7	56	105	24	29	153	56	39	201	46	72	249	48	34	297	50	42	345	60	71
10	21	67	58	7	29	106	24	46	154	56	59	202	46	71	250	48	60	298	50	20	346	60	55
11	21	48	59	7	46	107	24	64	155	56	50	203	46	55	251	48	52	299	50	47	347	60	42
12	21	39	60	7	64	108	24	67	156	56	53	204	46	42	252	48	72	300	50	49	348	60	20
13	21	59	61	7	67	109	24	48	157	56	25	205	46	20	253	48	71	301	53	25	349	60	47
14	21	50	62	7	48	110	24	39	158	56	68	206	46	47	254	48	55	302	53	68	350	60	49
15	21	53	63	7	39	111	24	59	159	56	34	207	46	49	255	48	42	303	53	34	351	52	72
16	21	25	64	7	59	112	24	50	160	56	60	208	64	67	256	48	20	304	53	60	352	52	71
17	21	68	65	7	50	113	24	53	161	56	52	209	64	48	257	48	47	305	53	52	353	52	55
18	21	34	66	7	53	114	24	25	162	56	72	210	64	39	258	48	49	306	53	72	354	52	42
19	21	60	67	7	25	115	24	68	163	56	71	211	64	59	259	39	59	307	53	71	355	52	20
20	21	52	68	7	68	116	24	34	164	56	55	212	64	50	260	39	50	308	53	55	356	52	47
21	21	72	69	7	34	117	24	60	165	56	42	213	64	53	261	39	53	309	53	42	357	52	49
22	21	71	70	7	60	118	24	52	166	56	20	214	64	25	262	39	25	310	53	20	358	72	71
23	21	55	71	7	52	119	24	72	167	56	47	215	64	68	263	39	68	311	53	47	359	72	55
24	21	42	72	7	72	120	24	71	168	56	49	216	64	34	264	39	34	312	53	49	360	72	42
25	21	20	73	7	71	121	24	55	169	29	46	217	64	60	265	39	60	313	25	68	361	72	20
26	21	47	74	7	55	122	24	42	170	29	64	218	64	52	266	39	52	314	25	34	362	72	47
27	21	49	75	7	42	123	24	20	171	29	67	219	64	72	267	39	72	315	25	60	363	72	49
28	17	7	76	7	20	124	24	47	172	29	48	220	64	71	268	39	71	316	25	52	364	71	55
29	17	23	77	7	47	125	24	49	173	29	39	221	64	55	269	39	55	317	25	72	365	71	42
30	17	24	78	7	49	126	38	56	174	29	59	222	64	42	270	39	42	318	25	71	366	71	20
31	17	38	79	23	24	127	38	29	175	29	50	223	64	20	271	39	20	319	25	55	367	71	47
32	17	56	80	23	38	128	38	46	176	29	53	224	64	47	272	39	47	320	25	42	368	71	49
33	17	29	81	23	56	129	38	64	177	29	25	225	64	49	273	39	49	321	25	20	369	55	42
34	17	46	82	23	29	130	38	67	178	29	68	226	67	48	274	59	50	322	25	47	370	55	20
35	17	64	83	23	46	131	38	48	179	29	34	227	67	39	275	59	53	323	25	49	371	55	47
36	17	67	84	23	64	132	38	39	180	29	60	228	67	59	276	59	25	324	68	34	372	55	49
37	17	48	85	23	67	133	38	59	181	29	52	229	67	50	277	59	68	325	68	60	373	42	20
38	17	39	86	23	48	134	38	50	182	29	72	230	67	53	278	59	34	326	68	52	374	42	47
39	17	59	87	23	39	135	38	53	183	29	71	231	67	25	279	59	60	327	68	72	375	42	49
40	17	50	88	23	59	136	38	25	184	29	55	232	67	68	280	59	52	328	68	71	376	20	47
41	17	53	89	23	50	137	38	68	185	29	42	233	67	34	281	59	72	329	68	55	377	20	49
42	17	25	90	23	53	138	38	34	186	29	20	234	67	60	282	59	71	330	68	42	378	47	49
43	17	68	91	23	25	139	38	60	187	29	47	235	67	52	283	59	55	331	68	20			
44	17	34	92	23	68	140	38	52	188	29	49	236	67	72	284	59	42	332	68	47			
45	17	60	93	23	34	141	38	72	189	46	64	237	67	71	285	59	20	333	68	49			
46	17	52	94	23	60	142	38	71	190	46	67	238	67	55	286	59	47	334	34	60			
47	17	72	95	23	52	143	38	55	191	46	48	239	67	42	287	59	49	335	34	52			
48	17	71	96	23	72	144	38	42	192	46	39	240	67	20	288	50	53	336	34	72			

Figure A3. The connections between the brain regions R1 and R2 corresponding to FNC features.

SVMRFE		RFFS1		RFFS2		SVMRFE		RFFS1		RFFS2	
Fea	Fre	Fea	Fre	Fea	Fre	Fea	Fre	Fea	Fre	Fea	Fre
26	20	11	20	7	20	17	12	25	11	19	12
30	20	26	20	11	20	22	12	31	10	31	12
6	19	24	19	16	20	29	12	9	8	18	11
11	19	30	19	24	20	5	11	12	8	17	10
7	18	7	18	26	20	13	11	14	6	20	10
32	18	32	18	30	20	16	11	17	5	21	10
24	17	16	17	32	20	20	10	28	4	1	9
19	16	29	17	12	19	28	10	1	3	8	9
3	16	3	17	29	18	2	9	5	3	27	9
23	15	2	16	3	18	4	8	8	2	23	7
14	14	4	15	25	16	25	8	13	2	13	6
21	14	19	14	2	15	27	8	15	2	5	5
31	14	10	13	4	15	1	7	18	2	9	4
9	13	6	13	10	14	15	7	20	1	14	4
10	13	21	13	22	13	18	6	22	1	15	2
12	12	23	12	6	12	8	5	27	1	28	1

Figure A4. SVMRFE and RFFS results of SBM data, where Fea represents the feature number and Fre represents the frequency at which the feature appears in 20 experiments.

SVMRFE		RFFS1		RFFS2		SVMRFE		RFFS1		RFFS2		SVMRFE		RFFS1		RFFS2	
Fea	Fre	Fea	Fre	Fea	Fre	Fea	Fre	Fea	Fre	Fea	Fre	Fea	Fre	Fea	Fre	Fea	Fre
13	20	244	20	5	20	278	19	71	14	321	20	152	16	42	8	47	17
18	20	295	20	13	20	279	19	89	14	328	20	158	16	68	8	54	17
20	20	226	20	30	20	313	19	106	14	333	20	162	16	69	8	96	17
40	20	302	20	33	20	328	19	142	14	353	20	199	16	81	8	106	17
42	20	37	19	37	20	332	19	156	13	68	19	305	16	85	8	151	17
43	20	183	19	40	20	352	19	173	13	83	19	329	16	98	8	170	17
48	20	220	19	48	20	356	19	245	13	128	19	338	16	102	8	182	17
79	20	243	19	61	20	361	19	251	13	142	19	340	16	119	8	215	17
83	20	33	19	62	20	371	19	259	13	165	19	341	16	148	8	228	17
102	20	289	19	63	20	372	19	304	12	190	19	345	16	157	8	256	17
106	20	61	19	64	20	45	18	321	12	194	19	24	15	169	8	296	17
138	20	292	19	71	20	147	18	5	11	210	19	38	15	170	8	298	17
177	20	62	19	75	20	182	18	30	11	211	19	59	15	172	8	312	17
181	20	64	19	78	20	185	18	90	11	251	19	61	15	181	8	325	17
183	20	189	18	85	20	215	18	125	11	278	19	62	15	182	8	342	17
189	20	297	18	102	20	219	18	208	11	301	19	70	15	190	8	16	16
213	20	63	18	105	20	233	18	222	11	304	19	125	15	193	8	38	16
234	20	78	18	135	20	251	18	277	11	318	19	194	15	198	8	113	16
243	20	185	18	150	20	254	18	278	11	335	19	198	15	200	7	157	16
244	20	290	18	156	20	256	18	293	11	337	19	200	15	209	7	163	16
265	20	279	18	171	20	342	18	312	11	339	19	289	15	232	7	169	16
270	20	211	18	173	20	29	17	323	10	350	19	299	15	233	7	172	16
275	20	40	18	183	20	57	17	368	10	368	19	322	15	234	7	233	16
276	20	328	17	185	20	89	17	4	10	376	19	373	15	242	7	235	16
285	20	353	17	189	20	100	17	41	10	4	18	2	14	246	7	264	16
295	20	165	17	208	20	118	17	45	10	9	18	8	14	248	7	275	16
301	20	337	17	213	20	144	17	49	10	20	18	110	14	255	7	323	16
337	20	48	17	220	20	190	17	51	10	29	18	124	14	257	7	334	16
339	20	150	16	221	20	193	17	54	10	42	18	171	14	264	7	347	16
353	20	171	16	226	20	201	17	88	10	43	18	179	14	268	7	356	16
5	19	265	16	243	20	238	17	118	10	45	18	232	14	274	7	49	15
33	19	333	16	244	20	292	17	128	10	89	18	235	14	275	7	88	15
37	19	13	16	265	20	311	17	144	10	118	18	242	14	276	7	205	15
75	19	221	16	279	20	312	17	210	9	138	18	262	14	306	7	232	15
78	19	9	15	284	20	331	17	213	9	179	18	277	14	309	7	236	15
165	19	29	15	289	20	334	17	253	9	200	18	282	14	318	7	245	15
211	19	38	15	290	20	363	17	334	9	219	18	293	14	319	7	276	15
220	19	47	15	292	20	1	16	335	9	257	18	300	14	340	7	307	15
259	19	194	15	293	20	96	16	373	9	259	18	308	14	342	7	363	15
269	19	219	15	295	20	98	16	15	9	285	18	333	14	343	7	15	14
272	19	284	14	297	20	140	16	20	8	35	17	368	14	344	7	23	14
273	19	339	14	302	20	142	16	39	8	41	17	19	13	359	7	107	14

Figure A5. SVMRFE and RFFS results of FNC data, Part 1.

SVMRFE		RFFS1		RFFS2		SVMRFE		RFFS1		RFFS2		SVMRFE		RFFS1		RFFS2	
Fea	Fre	Fea	Fre	Fea	Fre	Fea	Fre	Fea	Fre	Fea	Fre	Fea	Fre	Fea	Fre	Fea	Fre
30	13	367	7	108	14	247	11	282	5	26	11	216	9	92	2	178	9
41	13	370	7	137	14	250	11	283	5	46	11	221	9	95	2	184	9
56	13	375	7	161	14	260	11	287	5	51	11	236	9	96	2	216	9
60	13	8	6	167	14	288	11	291	5	69	11	253	9	99	2	274	9
132	13	23	6	181	14	290	11	296	5	72	11	291	9	103	2	319	9
157	13	26	6	193	14	298	11	299	5	90	11	307	9	104	2	349	9
188	13	34	6	209	14	302	11	307	5	124	11	316	9	108	2	370	9
210	13	44	6	223	14	306	11	311	4	125	11	324	9	109	2	7	8
268	13	58	6	329	14	375	11	316	4	133	11	349	9	110	2	55	8
297	13	67	6	330	14	23	10	320	4	180	11	366	9	111	2	57	8
304	13	73	6	371	14	25	10	322	4	234	11	12	8	116	2	76	8
318	13	75	6	11	13	93	10	338	4	255	11	26	8	120	2	116	8
325	13	83	6	95	13	139	10	347	4	294	11	34	8	121	2	134	8
336	13	93	6	112	13	143	10	350	4	299	11	35	8	122	2	136	8
50	12	97	6	191	13	175	10	355	4	311	11	73	8	126	2	192	8
54	12	100	6	248	13	180	10	357	4	340	11	99	8	127	2	197	8
55	12	107	6	253	13	196	10	363	4	344	11	117	8	133	2	250	8
58	12	113	5	260	13	202	10	365	4	345	11	129	8	135	2	271	8
71	12	115	5	277	13	212	10	372	4	365	11	145	8	136	2	287	8
127	12	123	5	282	13	225	10	376	4	373	11	191	8	138	2	308	8
141	12	130	5	291	13	227	10	2	4	375	11	197	8	147	2	316	8
148	12	131	5	313	13	230	10	3	4	34	10	209	8	155	2	361	8
218	12	137	5	315	13	263	10	6	4	44	10	214	8	158	2	367	8
223	12	141	5	22	12	280	10	11	4	81	10	229	8	160	2	8	7
357	12	145	5	39	12	309	10	12	3	82	10	255	8	161	2	58	7
14	11	151	5	66	12	315	10	17	3	130	10	266	8	163	2	103	7
17	11	152	5	109	12	346	10	18	3	222	10	294	8	164	2	104	7
51	11	159	5	114	12	354	10	21	3	238	10	296	8	167	2	111	7
63	11	162	5	127	12	4	9	31	3	239	10	344	8	177	2	145	7
64	11	166	5	131	12	6	9	32	3	242	10	351	8	179	2	146	7
68	11	168	5	144	12	9	9	35	3	249	10	355	8	184	2	155	7
112	11	176	5	186	12	28	9	36	3	273	10	378	8	186	2	158	7
167	11	180	5	198	12	46	9	43	3	305	10	49	7	187	2	164	7
169	11	199	5	212	12	47	9	46	3	306	10	65	7	195	2	176	7
173	11	215	5	225	12	76	9	50	2	372	10	69	7	202	1	214	7
205	11	216	5	246	12	95	9	53	2	36	9	77	7	204	1	229	7
207	11	238	5	263	12	101	9	56	2	50	9	85	7	205	1	262	7
208	11	241	5	288	12	119	9	72	2	86	9	91	7	207	1	268	7
226	11	256	5	309	12	170	9	76	2	139	9	116	7	212	1	269	7
231	11	260	5	358	12	184	9	82	2	141	9	126	7	217	1	270	7
237	11	262	5	374	12	203	9	84	2	159	9	146	7	218	1	272	7
239	11	263	5	6	11	204	9	87	2	175	9	176	7	230	1	300	7

Figure A6. SVMRFE and RFFS results of FNC data, Part 2.

SVMRFE		RFFS1		RFFS2		SVMRFE		RFFS1		RFFS2		SVMRFE		RFFS1		RFFS2	
Fea	Fre	Fea	Fre	Fea	Fre	Fea	Fre	Fea	Fre	Fea	Fre	Fea	Fre	Fea	Fre	Fea	Fre
186	7	231	1	320	7	108	5	7	0	2	4	3	3	175	0	207	2
195	7	235	1	327	7	111	5	10	0	52	4	31	3	178	0	224	2
217	7	237	1	343	7	113	5	14	0	70	4	36	3	188	0	240	2
241	7	239	1	351	7	121	5	16	0	73	4	52	3	191	0	241	2
248	7	240	1	14	6	131	5	19	0	80	4	80	3	192	0	258	2
258	7	249	1	17	6	133	5	22	0	94	4	82	3	196	0	283	2
267	7	250	1	24	6	137	5	24	0	140	4	84	3	197	0	310	2
274	7	254	1	28	6	149	5	25	0	147	4	92	3	201	0	331	2
283	7	258	1	93	6	150	5	27	0	154	4	105	3	203	0	338	2
284	7	266	1	100	6	156	5	28	0	166	4	120	3	206	0	348	2
286	7	267	1	115	6	159	5	52	0	177	4	123	3	214	0	364	2
319	7	269	1	152	6	160	5	55	0	187	4	128	3	223	0	369	2
350	7	270	1	188	6	163	5	57	0	203	4	134	3	224	0	378	2
376	7	281	1	201	6	166	5	59	0	247	4	136	3	225	0	18	1
377	7	285	1	227	6	192	5	60	0	280	4	164	3	227	0	56	1
7	6	286	1	261	6	246	5	65	0	354	4	245	3	228	0	79	1
15	6	288	1	267	6	281	5	66	0	377	4	249	3	229	0	87	1
27	6	298	1	324	6	303	5	70	0	19	3	257	3	236	0	97	1
39	6	301	1	346	6	317	5	74	0	27	3	264	3	247	0	99	1
66	6	303	1	360	6	348	5	77	0	32	3	287	3	252	0	120	1
87	6	305	1	362	6	369	5	79	0	84	3	327	3	261	0	121	1
104	6	313	1	12	5	370	5	80	0	92	3	360	3	271	0	143	1
107	6	314	1	31	5	374	5	86	0	110	3	362	3	272	0	148	1
114	6	315	1	60	5	10	4	91	0	122	3	365	3	273	0	160	1
135	6	317	1	65	5	21	4	94	0	126	3	367	3	280	0	196	1
151	6	325	1	74	5	22	4	101	0	129	3	11	2	294	0	231	1
154	6	329	1	98	5	32	4	105	0	168	3	44	2	300	0	266	1
161	6	330	1	101	5	81	4	112	0	206	3	53	2	308	0	326	1
172	6	341	1	117	5	88	4	114	0	252	3	67	2	310	0	341	1
178	6	346	1	119	5	122	4	117	0	281	3	72	2	324	0	357	1
187	6	348	1	174	5	130	4	124	0	314	3	97	2	326	0	1	0
206	6	349	1	195	5	155	4	129	0	332	3	103	2	327	0	3	0
240	6	351	1	204	5	168	4	132	0	10	2	153	2	331	0	77	0
261	6	354	1	218	5	174	4	134	0	21	2	224	2	332	0	123	0
320	6	358	1	237	5	222	4	139	0	25	2	228	2	336	0	132	0
323	6	360	1	254	5	271	4	140	0	53	2	252	2	345	0	153	0
347	6	361	1	303	5	310	4	143	0	59	2	326	2	352	0	202	0
359	6	362	1	317	5	314	4	146	0	67	2	358	2	356	0	217	0
16	5	364	1	322	5	321	4	149	0	91	2	86	1	366	0	230	0
74	5	369	1	352	5	335	4	153	0	149	2	109	1	371	0	286	0
90	5	378	1	355	5	343	4	154	0	162	2	115	1	374	0	336	0
94	5	1	0	359	5	364	4	174	0	199	2	330	1	377	0	366	0

Figure A7. SVMRFE and RFFS results of FNC data, Part 3.

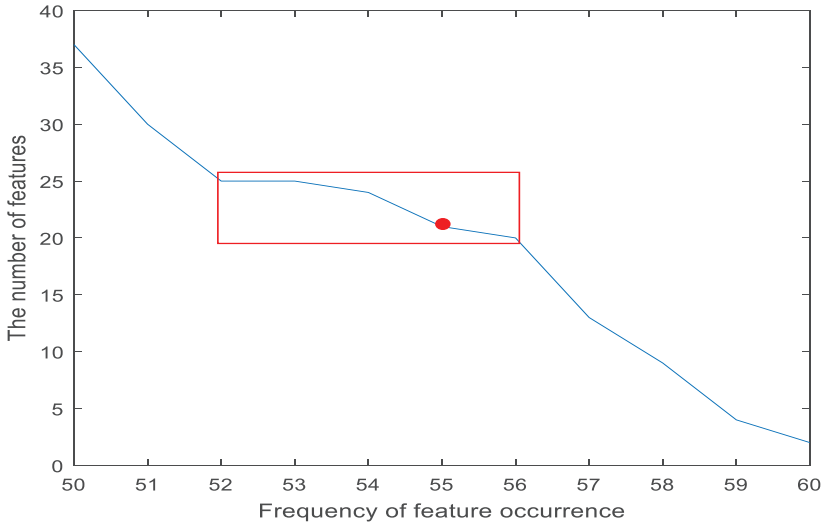

Figure A8. The characteristic frequency distribution with a frequency greater than or equal to 50. The *x* axis corresponds to the frequency of occurrence, and the *y* axis is the number of features. We can find that when the frequency is in the red range, i.e., greater than or equal to 52 and less than or equal to 56, the number of features is quite stable. Compared with other ranges, in the red range, there exists a balance between the number of features and the frequency of occurrence, which facilitates the abnormal analysis of brain function connections and structures corresponding to diseases. Therefore, we selected features with a frequency greater than or equal to 55.

References

1. Sui, J.; Qi, S.; van Erp, T.G.M.; Bustillo, J.; Jiang, R.; Lin, D.; Turner, J.A.; Damaraju, E.; Mayer, A.R.; Cui, Y.; et al. Multimodal neuromarkers in schizophrenia via cognition-guided MRI fusion. *Nat. Commun.* **2018**, *9*, 3028. [CrossRef] [PubMed]
2. Mp, V.D.H.; Fornito, A. Brain networks in schizophrenia. *Neuropsychol. Rev.* **2014**, *24*, 32–48. [CrossRef]
3. Woo, C.W.; Chang, L.J.; Lindquist, M.A.; Wager, T.D. Building better biomarkers: Brain models in translational neuroimaging. *Nat. Neurosci.* **2017**, *20*, 365–377. [CrossRef] [PubMed]
4. Du, Y.; Fryer, S.L.; Fu, Z.; Lin, D.; Sui, J.; Chen, J.; Damaraju, E.; Mennigen, E.; Stuart, B.; Mathalon, D.H.J.N. Dynamic functional connectivity impairments in early schizophrenia and clinical high-risk for psychosis. *NeuroImage* **2018**, *180*, 632–645. [CrossRef]
5. Shine, J.M.; Bissett, P.G.; Bell, P.T.; Koyejo, O.; Balsters, J.H.; Gorgolewski, K.J.; Moodie, C.A.; Poldrack, R.A. The dynamics of functional brain networks: Integrated network states during cognitive task performance. *Neuron* **2016**, *92*, 544–554. [CrossRef]
6. Rosenberg, M.D.; Finn, E.S.; Scheinost, D.; Papademetris, X.; Shen, X.; Constable, R.T.; Chun, M.M. A neuromarker of sustained attention from wholebrain functional connectivity. *Nat. Neurosci.* **2016**, *19*, 165–171. [CrossRef]
7. Finn, E.S; Shen, X.; Scheinost, D.; Rosenberg, M.D.; Huang, J.; Chun, M.M.; Papademetris, X.; Constable, R.T. Functional connectome fingerprinting: Identifying individuals using patterns of brain connectivity. *Nat. Neurosci.* **2015**, *18*, 1664–1671. [CrossRef] [PubMed]
8. Palaniyappan, L.; Mahmood, J.; Balain, V.; et al. Structural correlates of formal thought disorder in schizophrenia: An ultra-high field multivariate morphometry study. *Schizophr. Res.* **2015**, *168*, 305–312. [CrossRef]
9. Kong, Y.; Yu, T. A graph-embedded deep feedforward network for disease outcome classification and feature selection using gene expression data. *Bioinformatics* **2018**, *34*, 3727–3737. [CrossRef] [PubMed]
10. Suk, H.I.; Lee, S.W.; Shen, D. Deep ensemble learning of sparse regression models for brain disease diagnosis. *Med. Image Anal.* **2017**, *37*, 101–113. [CrossRef]
11. Demirhan, A. The effect of feature selection on multivariate pattern analysis of structural brain MR images. *Phys. Med.* **2018**, *47*, 103–111. [CrossRef]

12. Cao, F.; Liu, Y.; Wang, D. Efficient Saliency Detection Using Convolutional Neural Networks with Feature Selection. *Inf. Sci.* **2018**, *456*, 34–49. [CrossRef]
13. Liu, Z.T.; Wu, M.; Cao, W.H.; Mao, J.W.; Tan, G.Z. Speech emotion recognition based on feature selection and extreme learning machine decision tree. *Neurocomputing* **2018**, *273*, 271–280. [CrossRef]
14. Chandrashekar, G.; Sahin, F. A survey on feature selection methods. *Comput. Electr. Eng.* **2014**, *40*, 16–28. [CrossRef]
15. Lazar, C.; Taminau, J.; Meganck, S.; Steenhoff, D.; Coletta, A.; Molter, C.; De, S.V.; Duque, R.; Bersini, H.; Nowé, A. A survey on filter techniques for feature selection in gene expression microarray analysis. IEEE/ACM Trans. *Comput. Biol. Bioinform.* **2012**, *9*, 1106–1119. [CrossRef]
16. Foithong, S.; Pinngern, O.; Attachoo, B. Feature subset selection wrapper based on mutual information and rough sets. *Expert Syst. Appl.* **2012**, *39*, 574–584. [CrossRef]
17. Cadenas, J.M.; Garrido, M.C.; Martínez, R. Feature subset selection Filter-Wrapper based on low quality data. *Expert Syst. Appl.* **2013**, *40*, 6241–6252. [CrossRef]
18. Shen, Q.; Diao, R.; Su, P. Feature Selection Ensemble. *Turing 100*, **2012**, *10*, 289–306.
19. Lu, H.; Chen, J.; Yan, K.; Jin, Q.; Xue, Y.; Gao, Z. A hybrid feature selection algorithm for gene expression data classification. *Neurocomputing* **2017**, *256*, 56–62. [CrossRef]
20. Zhe, F.L. A Novel Hybrid Feature Selection Methods and Prediction for Ready Biodegradibility of Chemicals Using Random Forests and Boruta. In Proceedings of the 8th International Conference on Researches in Engineering, Technology and Sciences (ICRETS), Istanbul, Turkey, 13–14 August 2015.
21. Lyu, H.; Wan, M.; Han, J.; Liu, R.; Wang, C. A filter feature selection method based on the Maximal Information Coefficient and Gram-Schmidt Orthogonalization for biomedical data mining. *Comput. Biol. Med.* **2017**, *89*, 264–274. [CrossRef]
22. Zhang, X.; Zhang, Q.; Miao, C.; Sun, Y.; Qin, X.; Li, H. A two-stage feature selection and intelligent fault diagnosis method for rotating machinery using hybrid Filter and Wrapper method. *Neurocomputing* **2017**, *275*, 2426–2439. [CrossRef]
23. Moon, M.; Nakai, K. Stable feature selection based on the ensemble *L*1-norm support vector machine for biomarker discovery. *BMC Genom.* **2016**, *17*, 1026. [CrossRef] [PubMed]
24. Chen, Y.; Yang, W.; Long, J.; Zhang, Y.; Feng, J.; Li, Y.; Huang, B. Discriminative analysis of Parkinson's disease based on whole-brain functional connectivity. *PLoS ONE* **2015**, *10*, e0124153. [CrossRef] [PubMed]
25. Zeng, L.L.; Shen, H.; Liu, L.; Wang, L.; Li, B.; Fang, P.; Zhou, Z.; Li, Y.; Hu, D. Identifying major depression using whole-brain functional connectivity: A multivariate pattern analysis. *Brain J. Neurol.* **2012**, *135*, 1498–1507. [CrossRef]
26. Haznedar, M.M.; Buchsbaum, M.S.; Hazlett, E.A.; Shihabuddin, L.; New, A.; Siever, L.J. Cingulate gyrus volume and metabolism in the schizophrenia spectrum. *Schizophr. Res.* **2004**, *71*, 249–262. [CrossRef]
27. Calabrese, D.R.; Wang, L.; Harms, M.P.; Ratnanather, J.T.; Barch, D.M.; Cloninger, C.R.; Thompson, P.A.; Miller, M.I.; Csernansky, J.G. Cingulate gyrus neuroanatomy in schizophrenia subjects and their non-psychotic siblings. *Schizophr. Res.* **2008**, *104*, 61–70. [CrossRef] [PubMed]
28. Shah, C.; Zhang, W.; Xiao, Y.; Yao, L.; Zhao, Y.; Gao, X.; Liu, L.; Liu, J.; Li, S.; Tao, B. Common pattern of gray-matter abnormalities in drug-naive and medicated first-episode schizophrenia: A multimodal meta-analysis. *Psychol. Med.* **2016**, *47*, 401–413. [CrossRef]
29. Chang, M.; Womer, F.Y.; Bai, C.; Zhou, Q.; Wei, S.; Jiang, X.; Geng, H.; Zhou, Y.; Tang, Y.; Wang, F. Voxel-Based Morphometry in Individuals at Genetic High Risk for Schizophrenia and Patients with Schizophrenia during Their First Episode of Psychosis. *PLoS ONE* **2016**, *11*, e0163749. [CrossRef]
30. Liang, M.; Zhou, Y.; Jiang, T.; Liu, Z.; Tian, L.; Liu, H.; Hao, Y. Widespread functional disconnectivity in schizophrenia with resting-state functional magnetic resonance imaging. *Neuroreport* **2006**, *17*, 209–213. [CrossRef]
31. Xu, Y.; Qin, W.; Zhuo, C.; Xu, L.; Zhu, J.; Liu, X.; Yu, C. Selective functional disconnection of the orbitofrontal subregions in schizophrenia. *Psychol. Med.* **2017**, *47*, 1637–1646. [CrossRef]
32. Zhang, D.; Guo, L.; Hu, X.; Li, K.; Zhao, Q.; Liu, T. Increased cortico-subcortical functional connectivity in schizophrenia. *Brain Imaging Behav.* **2012**, *6*, 27–35. [CrossRef] [PubMed]
33. Guyon, I.; Weston, J.; Barnhill, S.; Vapnik, V. Gene Selection for Cancer Classification using Support Vector Machines. *Mach. Learn.* **2002**, *46*, 389–422. [CrossRef]

34. Martino, F.D.; Valente, G.; Staeren, N.; Ashburner, J.; Goebel, R.; Formisano, E. Combining multivariate voxel selection and support vector machines for mapping and classification of fMRI spatial patterns. *NeuroImage* **2008**, *43*, 44–58. [CrossRef] [PubMed]
35. You, W.; Yang, Z.; Ji, G. PLS-based recursive feature elimination for high-dimensional small sample. *Knowl.-Based Syst.* **2014**, *55*, 15–28. [CrossRef]
36. Yan, K.; Zhang, D. Feature selection and analysis on correlated gas sensor data with recursive feature elimination. *Sens. Actuators B Chem.* **2015**, *212*, 353–363. [CrossRef]
37. Huang, M.L.; Hung, Y.H.; Lee, W.M.; Li, R.K.; Jiang, B.R. SVM-RFE based feature selection and Taguchi parameters optimization for multiclass SVM classifier. *Sci. World J.* **2014**, *2014*, 795624. [CrossRef] [PubMed]
38. Kumar, A.; Sharmila, D.J.S.; Singh, S. SVMRFE based approach for prediction of most discriminatory gene target for type II diabetes. *Genom. Data* **2017**, *12*, 28–37. [CrossRef] [PubMed]
39. Ho, T.K. Random Decision Forests. In *Encyclopedia of Machine Learning*; Sammut, C., Webb, G.I., Eds.; Springer: Boston, MA, USA, 2010; p. 827.
40. Breiman, L. Random Forests. *Mach. Learn.* **2001**, *45*, 5–32. [CrossRef]
41. Rahman, M.S.; Rahman, M.K.; Kaykobad, M.; Rahman, M.S. isGPT: An optimized model to identify sub-Golgi protein types using SVM and Random Forest based feature selection. *Artif. Intell. Med.* **2017**, *84*, 90–100. [CrossRef]
42. Zhou, Q.; Hao, Z.; Zhou, Q.; Fan, Y.; Luo, L. Structure damage detection based on random forest recursive feature elimination. *Mech. Syst. Signal Process.* **2014**, *46*, 82–90. [CrossRef]
43. Yao, D.J.; Yang, J.; Zhan, X.J. Feature selection algorithm based on random forest. *J. Jilin Univ.* **2014**, *44*, 137–141. [CrossRef]
44. Nanthagopal, A.P.; Sukanesh, R. Wavelet statistical texture features-based segmentation and classification of brain computed tomography images. *IET Image Process.* **2013**, *7*, 25–32. [CrossRef]
45. Mehlhorn, H.; Schreiber, F. Small-World Property. In *Encyclopedia of Systems Biology*; Dubitzky, W., Wolkenhauer, O., Cho, K.-H., Yokota, H., Eds.; Springer: New York, NY, USA, 2013; pp. 1957–1959.
46. Mittal, V.A.; Walker, E.F. Diagnostic and Statistical Manual of Mental Disorders. *Psychiatry Res.* **2011**, *189*, 158–159. [CrossRef]
47. Segall, J.M.; Allen, E.A.; Jung, R.E.; Erhardt, E.B.; Arja, S.K.; Kiehl, K.; Calhoun, V.D. Correspondence between structure and function in the human brain at rest. *Front. Neuroinform.* **2012**, *6*, 10. [CrossRef]
48. Allen, E.A.; Erhardt, E.B.; Damaraju, E.; Gruner, W.; Segall, J.M.; Silva, R.F.; Havlicek, M.; Rachakonda, S.; Fries, J.; Kalyanam, R.; et al. A baseline for the multivariate comparison of resting-state networks. *Front. Syst. Neurosci.* **2011**, *5*, 2. [CrossRef]
49. Xia, M.; Wang, J.; He, Y. BrainNet Viewer: A network visualization tool for human brain connectomics. *PLoS ONE* **2013**, *8*, e68910. [CrossRef]
50. Xia, M.; Womer, F.Y.; Chang, M.; Zhu, Y.; Zhou, Q.; Edmiston, E.K.; Jiang, X.; Wei, S.; Duan, J.; Xu, K. Shared and Distinct Functional Architectures of Brain Networks Across Psychiatric Disorders. *Schizophr. Bull.* **2018**, *45*, 450–463. [CrossRef]
51. Yong, L.; Meng, L.; Yuan, Z.; Yong, H.; Yihui, H.; Ming, S.; Chunshui, Y.; Haihong, L.; Zhening, L.; Tianzi, J. Disrupted small-world networks in schizophrenia. *Brain* **2008**, *131*, 945–961. [CrossRef]
52. Benes, F.M. Evidence for neurodevelopment disturbances in anterior cingulate cortex of post-mortem schizophrenic brain. *Schizophr. Res.* **1991**, *5*, 187–188. [CrossRef]
53. Mirjalili, M.; Hossein-Zadeh, G.-A. Characterization of schizophrenia by linear kernel canonical correlation analysis of resting-state functional MRI and structural MRI. In Proceedings of the 2017 7th International Conference on Computer and Knowledge Engineering (ICCKE), Mashhad, Iran, 26–27 October 2017; pp. 37–41.
54. Calderone, D.J.; Hoptman, M.J.; Antígona, M.; Sangeeta, N.C.; Mauro, C.J.; Moshe, B.; Javitt, D.C.; Butler, P.D. Contributions of low and high spatial frequency processing to impaired object recognition circuitry in schizophrenia. *Cerebr. Cortex* **2013**, *23*, 1849–1858. [CrossRef]
55. Susan, W.G.; Thermenos, H.W.; Snezana, M.; Tsuang, M.T.; Faraone, S.V.; Mccarley, R.W.; Shenton, M.E.; Green, A.I.; Alfonso, N.C.; Peter, L.V.; et al. Hyperactivity and hyperconnectivity of the default network in schizophrenia and in first-degree relatives of persons with schizophrenia. *Proc. Natl. Acad. Sci. USA* **2009**, *106*, 1279–1284. [CrossRef]

56. Corr, P.J. Reinforcement sensitivity theory and personality. *Neurosci. Biobehav. Rev.* **2004**, *28*, 317–332. [CrossRef] [PubMed]
57. Jylhä, P.; Isometsä, E. Temperament, character and symptoms of anxiety and depression in the general population. *Eur. Psychiatry* **2006**, *21*, 389–395. [CrossRef]
58. Van Schuerbeek, P.; Baeken, C.; De Raedt, R.; De Mey, J.; Luypaert, R. Individual differences in local gray and white matter volumes reflect differences in temperament and character: A voxel-based morphometry study in healthy young females. *Brain Res.* **2011**, *1371*, 32–42. [CrossRef] [PubMed]
59. Trimble, M. Molecular neuropharmacology, a foundation for clinical neuroscience. *Psychiatry* **2002**, *73*, 210. [CrossRef]
60. Qingbao, Y.; Allen, E.A.; Jing, S.; Arbabshirani, M.R.; Godfrey, P.; Calhoun, V.D. Brain connectivity networks in schizophrenia underlying resting state functional magnetic resonance imaging. *Curr. Top. Med. Chem.* **2012**, *12*, 2415–2425. [CrossRef]
61. Gaudio, S.; Wiemerslage, L.; Brooks, S.J.; Schiöth, H.B. A systematic review of resting-state functional-MRI studies in anorexia nervosa: Evidence for functional connectivity impairment in cognitive control and visuospatial and body-signal integration. *Neurosci. Biobehav. Rev.* **2016**, *71*, 578–589. [CrossRef]
62. Wu, C.; Zheng, Y.; Li, J.; Wu, H.; She, S.; Liu, S.; Ning, Y.; Li, L. Brain substrates underlying auditory speech priming in healthy listeners and listeners with schizophrenia. *Psychol. Med.* **2016**, *47*, 837–852. [CrossRef]
63. Qiu, L.; Yan, H.; Zhu, R.; Yan, J.; Yuan, H.; Han, Y.; Yue, W.; Tian, L.; Zhang, D. Correlations between exploratory eye movement, hallucination, and cortical gray matter volume in people with schizophrenia. *BMC Psychiatry* **2018**, *18*, 226. [CrossRef]
64. Viher, P.; Walther, S. SU67. Aberrant Resting-State Functional Connectivity in the Motor System and Motor Abnormalities in Schizophrenia. *Schizophr. Bull.* **2017**, *43*, S185–S186. [CrossRef]
65. Sha, Z.; Wager, T.D.; Mechelli, A.; He, Y. Common Dysfunction of Large-Scale Neurocognitive Networks Across Psychiatric Disorders. *Biol. Psychiatry* **2019**, *85*, 379–388. [CrossRef] [PubMed]
66. Anticevic, A.; Cole, M.W.; Murray, J.D.; Corlett, P.R.; Wang, X.-J.; Krystal, J.H. The role of default network deactivation in cognition and disease. *Trends Cogn. Sci.* **2012**, *16*, 584–592. [CrossRef] [PubMed]
67. Menon, V. Large-scale brain networks and psychopathology: A unifying triple network model. *Trends Cogn. Sci.* **2011**, *15*, 483–506. [CrossRef]
68. Wager, T.D.; Smith, E.E. Neuroimaging studies of working memory. *Cogn. Affect. Behav. Neurosci.* **2003**, *3*, 255–274. [CrossRef]
69. Wu, L.; Caprihan, A.; Bustillo, J.; Mayer, A.; Calhoun, V. An approach to directly link ICA and seed-based functional connectivity: Application to schizophrenia. *NeuroImage* **2018**, *179*, 448–470. [CrossRef]